

A HYBRID N -BODY CODE INCORPORATING ALGORITHMIC REGULARIZATION AND POST-NEWTONIAN FORCES

STEFAN HARFST

Sterrenkundig Instituut “Anton Pannekoek”, University of Amsterdam, Kruislaan 403, 1098SJ Amsterdam, The Netherlands

ALESSIA GUALANDRIS AND DAVID MERRITT

Center for Computational Relativity and Gravitation, Rochester Institute of Technology, 78 Lomb Memorial Drive, Rochester, NY 14623

SEPPO MIKKOLA

Tuorla Observatory, University of Turku, Väisäläntie 20, Piikkiö, Finland

Draft version May 28, 2019

ABSTRACT

We describe a novel N -body code designed for simulations of the central regions of galaxies containing massive black holes. The code incorporates Mikkola’s “algorithmic” chain regularization scheme including post-Newtonian terms up to PN2.5 order. Stars moving beyond the chain are advanced using a fourth-order integrator with forces computed on a GRAPE board. Performance tests confirm that the hybrid code achieves better energy conservation, in less elapsed time, than the standard scheme and that it reproduces the orbits of stars tightly bound to the black hole with high precision. The hybrid code is applied to two sample problems: the effect of finite- N gravitational fluctuations on the orbits of the S-stars; and inspiral of an intermediate-mass black hole into the galactic center.

Subject headings: Galaxy: centre – stellar dynamics – methods: N -body simulations

1. INTRODUCTION

Standard N -body integrators have difficulty reproducing the motion of tight binaries, or following close hyperbolic encounters between stars. Unless the integration time step is made very short, the relative orbit will not be accurately reproduced, and the system energy may also exhibit an unacceptable drift since a single compact subsystem can contain a large fraction of the total binding energy. This difficulty is particularly limiting for studies of the centers of galaxies like the Milky Way, where the gravitational potential is dominated by a (single or binary) supermassive black hole. Early attempts to simulate such systems often had difficulty achieving the required accuracy and performance (e.g. Sigurdsson et al. 1995). In later studies, stars in tightly bound orbits around the black hole were sometimes simply removed (e.g. Baumgardt et al. 2004; Matsubayashi et al. 2007); in other studies, the position and velocity of the most massive particle were artificially fixed and the stellar orbits approximated as perturbed Keplerian ellipses (e.g. Löckmann & Baumgardt 2008). While these approaches can be useful for certain problems, a less approximate treatment is indicated for studies in which the motion of stars near the black hole is used to constrain the magnitude of non-Keplerian perturbations (Fragile & Mathews 2000; Weinberg et al. 2005; Will 2008). Fixing the location of the most massive particle can also be problematic when simulating binary or multiple supermassive black holes.

Aarseth (2003b) summarizes the various regularized schemes that have been incorporated into N -body codes to treat strong gravitational interactions with high accuracy and without loss of performance.

(1) The KS-regularization method (Kustaanheimo & Stiefel 1965), together with the original chain method (Mikkola & Aarseth 1993) which uses the KS-transformation to regularize multiparticle systems, has been widely used to integrate binaries in simulations of star clusters. This method has also been applied to the binary black hole problem (e.g. Quinlan & Hernquist 1997; Milosavljević & Merritt 2001; Merritt et al. 2007). This approach suffers from inaccuracies when mass ratios are very large because the total energy that appears in the equations of motion is dominated by the binary (Aarseth 2003a).

(2) In the case of a single dominant body, an alternative to the chain geometry, called wheel-spoke (WS) regularization, treats each interaction with the massive body via the standard KS-regularization, while other interactions use a small softening to avoid singularities (Zare 1974; Aarseth 2007).

(3) Algorithmic regularization (AR) methods effectively remove singularities with a time transformation accompanied by the leapfrog algorithm. There are two such methods: the logarithmic Hamiltonian (LogH) (Mikkola & Tanikawa 1999b,a; Preto & Tremaine 1999) and time-transformed leapfrog (TTL) (Mikkola & Aarseth 2002). Both these algorithms produce exact trajectories for the unperturbed two-body problem and provide regular results for more general cases. In the LogH method the derivative of time is inversely proportional to the gravitational potential while in TTL the potential is replaced by the sum of all inverse distances. Contrary to the KS-chain, zero masses do not cause any singularity in these AR-methods; TTL even provides equal weight to all the members of the subsystem, and thus these methods are well suited for integration of systems with large mass ratios. Use of the gen-

eralized mid-point method (Mikkola & Merritt 2006) allows velocity-dependent terms, e.g. the post-Newtonian expansion. In addition to the leapfrog and/or generalized mid-point method one must use the Bulirsch-Stoer (BS) extrapolation method for high accuracy. The basic algorithms provide the correct symmetry for the BS method to work efficiently. In a recent implementation (Mikkola & Merritt 2007), called AR-CHAIN, the chain structure, introduced originally by Mikkola & Aarseth (1993), is incorporated with a new time-transformation that combines the advantages of the LogH and TTL and generalized mid-point methods. The chain structure significantly reduces the roundoff error and the other transformations provide regular data, necessary to achieve high precision, for the BS-extrapolator. The AR-CHAIN code also includes post-Newtonian terms to order PN2.5

In this paper we describe the performance of a new, hybrid N -body code that incorporates AR-CHAIN. The new code, called φ GRAPECH, is based on (the serial version of) φ GRAPE, a general-purpose, direct-summation N -body code which uses GRAPE special-purpose hardware to compute accelerations (Harfst et al. 2007). The new code divides particles into two groups: particles associated with the massive object (or objects) and that are included in the chain, and particles outside the chain that are advanced via the Hermite scheme of φ GRAPE. Some of the latter particles are denoted as perturbers and are allowed to affect the motion of stars in the chain, and vice versa. After describing the hybrid code (§2), we present the results of performance tests based on a model that mimics the star cluster around a supermassive black hole (§3). We show that the hybrid code can achieve higher overall accuracies (as measured via energy conservation, say) than φ GRAPE alone, and in less elapsed time, in spite of the additional overhead associated with the chain.

In §4 we apply φ GRAPECH to the integration of a realistic, multi-component model of the Galactic center. In the first application (§4.1) we accurately evaluate, for the first time, the effects of perturbations from stars and stellar remnants on the orbital elements of the S-stars (Eisenhauer et al. 2005; Ghez et al. 2005). We then (§4.2) present an integration of the orbit of an intermediate-mass black hole as it spirals into the galactic center via the combined influence of dynamical friction and gravitational-wave energy loss.

2. THE HYBRID N -BODY CODE

In this section we describe how the AR-CHAIN algorithm of Mikkola & Merritt (2007) was integrated into the serial version of the direct-summation code φ GRAPE (Harfst et al. 2007). The latter algorithm employs a Hermite integration scheme (Makino & Aarseth 1992) with hierarchical, commensurate block time steps and uses a GRAPE board to calculate forces.

We begin by briefly describing the integration scheme without the chain and its implementation using the GRAPE.

2.1. Integration scheme

In addition to position \mathbf{x}_i , velocity \mathbf{v}_i , acceleration \mathbf{a}_i , and time derivative of acceleration $\dot{\mathbf{a}}_i$, each particle i has its own time t_i and time step Δt_i .

Integration consists of the following steps:

- (1) The initial time steps are calculated from

$$\Delta t_i = \eta_s \frac{|\mathbf{a}_i|}{|\dot{\mathbf{a}}_i|}, \quad (1)$$

where typically $\eta_s = 0.01$ gives sufficient accuracy.

- (2) The system time t is set to the minimum of all $t_i + \Delta t_i$, and all particles i that have $t_i + \Delta t_i = t$ are selected as active particles.
- (3) Positions and velocities at the new t are predicted for all particles using

$$\begin{aligned} \mathbf{x}_{j,p} &= \mathbf{x}_{j,0} + (t - t_j)\mathbf{v}_{j,0} + \frac{(t - t_j)^2}{2}\mathbf{a}_{j,0} + \frac{(t - t_j)^3}{6}\dot{\mathbf{a}}_{j,0} \\ \mathbf{v}_{j,p} &= \mathbf{v}_{j,0} + (t - t_j)\mathbf{a}_{j,0} + \frac{(t - t_j)^2}{2}\dot{\mathbf{a}}_{j,0}. \end{aligned} \quad (2b)$$

Here, the second subscript denotes a value given either at the beginning (0) or the end (1) of the current time step. All quantities used in the predictor can be calculated directly, i.e. no memory of a previous time step is required.

- (4) Acceleration and its time derivative are updated for active particles only according to

$$\mathbf{a}_{i,1} = \sum_{j \neq i} Gm_j \frac{\mathbf{r}_{ij}}{(r_{ij}^2 + \epsilon^2)^{(3/2)}}, \quad (3a)$$

$$\dot{\mathbf{a}}_{i,1} = \sum_{j \neq i} Gm_j \left[\frac{\mathbf{v}_{ij}}{(r_{ij}^2 + \epsilon^2)^{(3/2)}} + \frac{3(\mathbf{v}_{ij} \cdot \mathbf{r}_{ij})\mathbf{r}_{ij}}{(r_{ij}^2 + \epsilon^2)^{(5/2)}} \right] \quad (3b)$$

where

$$\mathbf{r}_{ij} = \mathbf{x}_{j,p} - \mathbf{x}_{i,p}, \quad (4a)$$

$$\mathbf{v}_{ij} = \mathbf{v}_{j,p} - \mathbf{v}_{i,p}, \quad (4b)$$

and ϵ is the softening parameter.

- (5) Positions and velocities of active particles are corrected using

$$\mathbf{x}_{i,1} = \mathbf{x}_{i,p} + \frac{\Delta t_i^4}{24}\mathbf{a}_{i,0}^{(2)} + \frac{\Delta t_i^5}{120}\mathbf{a}_{i,0}^{(3)}, \quad (5a)$$

$$\mathbf{v}_{i,1} = \mathbf{v}_{i,p} + \frac{\Delta t_i^3}{6}\mathbf{a}_{i,0}^{(2)} + \frac{\Delta t_i^4}{24}\mathbf{a}_{i,0}^{(3)} \quad (5b)$$

where the second and third time derivatives of \mathbf{a} are given by

$$\mathbf{a}_{i,0}^{(2)} = \frac{-6(\mathbf{a}_{i,0} - \mathbf{a}_{i,1}) - \Delta t_i(4\dot{\mathbf{a}}_{i,0} + 2\dot{\mathbf{a}}_{i,1})}{\Delta t_i^2}, \quad (6a)$$

$$\mathbf{a}_{i,0}^{(3)} = \frac{12(\mathbf{a}_{i,0} - \mathbf{a}_{i,1}) + 6\Delta t_i(\dot{\mathbf{a}}_{i,0} + \dot{\mathbf{a}}_{i,1})}{\Delta t_i^3}. \quad (6b)$$

- (6) The times t_i are updated and the new time steps Δt_i are determined. Time steps are calculated using the standard formula (Aarseth 1985):

$$\Delta t_{i,1} = \sqrt{\eta \frac{|\mathbf{a}_{i,1}||\mathbf{a}_{i,1}^{(2)}| + |\dot{\mathbf{a}}_{i,1}|^2}{|\dot{\mathbf{a}}_{i,1}||\mathbf{a}_{i,1}^{(3)}| + |\mathbf{a}_{i,1}^{(2)}|^2}}. \quad (7)$$

The parameter η controls the accuracy of the integration and is typically set to 0.01 (although the use of smaller value of η is described below). The value of $\mathbf{a}_{i,1}^{(2)}$ is calculated from

$$\mathbf{a}_{i,1}^{(2)} = \mathbf{a}_{i,0}^{(2)} + \Delta t_{i,0} \mathbf{a}_{i,0}^{(3)} \quad (8)$$

and $\mathbf{a}_{i,1}^{(3)}$ is set to $\mathbf{a}_{i,0}^{(3)}$.

(7) Repeat from step (2).

A hierarchical commensurate block time step scheme is necessary when the Hermite integrator is used with the GRAPE (and is also efficient for parallelization and vectorization; see below and McMillan (1986)). Particles are grouped by replacing their time steps Δt_i with a block time step $\Delta t_{i,b} = (1/2)^n$, where n is chosen according to

$$\left(\frac{1}{2}\right)^n \leq \Delta t_i < \left(\frac{1}{2}\right)^{n-1}. \quad (9)$$

The commensurability is enforced by requiring that $t/\Delta t_i$ be an integer. For numerical reason we also set a minimum time step Δt_{\min} , where typically

$$\Delta t_{\min} = 2^{-m}, \quad (10)$$

with $m \geq 28$. The time steps of particles with $\Delta t_i < \Delta t_{\min}$ are set to this value. The minimum time step should be consistent with the maximum acceleration defined by the softening parameter; monitoring of the total energy can generally indicate whether this condition is being violated.

2.2. GRAPE implementation

The GRAPE-6 and GRAPE-6A hardware has been designed to work with a Hermite integration scheme and is therefore easily integrated into the algorithm described in the previous section (see Makino et al. 2003). In detail, integration of particle positions using the GRAPE-6A consists of the following steps:

- (1) **Initialize** the GRAPE and send particle data (positions, velocities, etc.) to GRAPE memory.
- (2) **Compute** the next system time t and select active particles on the host (same as step 2 in previous section).
- (3) **Predict** positions and velocities of active particles only and send the predicted values together with the new system time t to GRAPE's force calculation pipeline.
- (4) **Predict** positions and velocities for all other particles on the GRAPE, and calculate forces and their time derivatives for active particles.
- (5) **Retrieve** forces and their time derivatives from the GRAPE and **correct** positions and velocities of active particles on the host.

(6) **Compute** the new time steps and update the particle data on the host of all active particles in the GRAPE memory.

(7) **Repeat** from step (2).

2.3. Integrating AR-CHAIN into φ GRAPE

Here we describe the hybrid N -body code. We first describe the step-by-step algorithm as in the previous section, then provide a more detailed explanation of the most important steps.

- (1) **Initialize** the GRAPE and send particle data (positions, velocities, etc.) to GRAPE memory.
- (2) **Compute** the next system time t and select active particles on the host (same as step 2 in previous section).
- (3) If the chain is not active, **check** the active particles to see whether the chain should be used. If the chain is active, **check** if particles enter or leave the chain.
- (4) If the chain is not needed, standard integration can continue from step (14). Otherwise, **(re-)initialize** the chain if a new chain has been created or an existing chain has changed.
- (5) **Find** all particles within a sphere of radius r_{pert} centered on the center-of-mass (COM) chain particle and define them as perturbers.
- (6) **Compute** forces on the COM particle (if the chain is new or has changed).
- (7) **Evolve** the chain one time step.
- (8) **Predict** the position and velocity of the COM chain particle, **compute** forces and **correct** its position and velocity.
- (9) **Resolve** the chain and **update** positions and velocities of both the chain COM particle and the individual chain particles.
- (10) **Integrate** all active particles; particles within r_{res} feel the forces from the resolved chain (i.e. individual chain particles) and particles outside r_{res} feel only the forces from the chain COM particle.
- (11) **Compute** new time steps for the active particles.

- (12) **Update** the particle data on the host CPU and the GRAPE for all active particles.
- (13) **Repeat** from step (2).
- (14) **Predict** positions and velocities of active particles only and send the predicted values together with the new system time t to the GRAPE force calculation pipeline.
- (15) **Predict** positions and velocities for all other particles on the GRAPE, and calculate forces and their time derivatives for active particles.
- (16) **Retrieve** forces and their time derivatives from the GRAPE and **correct** positions and velocities of active particles on the host.
- (17) **Compute** the new time steps and update the particle data on the host of all active particles in the GRAPE memory.
- (18) **Repeat** from step (2).

In the remainder of this section, we describe in detail the implementation of the hybrid code. For purposes of discussion, we assume a test case where a very massive particle is located near the center of the system, e.g. a supermassive black hole in the galactic center. But the same algorithm can be easily applied to other configurations as well.

The hybrid code is initialized in the manner described above. After the time steps for all particles have been determined, a check is made whether to use the chain. Two parameters control the assignment of particles to the chain: t_{crit} and r_{crit} . Initially, any particle that satisfies both criteria:

$$\Delta t_i \leq t_{\text{crit}} \quad (11a)$$

$$\Delta r_{i,\text{BH}} \leq r_{\text{crit}} \quad (11b)$$

is selected as a chain particle, where $r_{i,\text{BH}}$ is the distance of particle i to the massive particle. Once the chain is activated and a chain radius (as defined below) is determined, all particles within r_{ch} are assigned to the chain, i.e. t_{crit} is ignored. If two or more particles are selected as chain particles the chain is activated; the massive particle is always designated a chain particle.

If the chain is not needed the code continues with the standard N -body integration. Otherwise a new chain is created (step 4). The chain radius r_{ch} is set to the largest $r_{i,\text{BH}}$ found in the previous step and all particles within r_{ch} are added to chain independent of their time step. Any chain particle with $t_i \neq t_{\text{sys}}$, where t_{sys} is the current system time, is integrated to this time. Then a pseudo chain particle is created with the COM coordinates of the chain particles. The chain particles are also removed from the list of active particles and their masses are set to zero on the GRAPE.

All particles within r_{pert} are selected as perturber particles (5) and the perturber radius is calculated from

$$r_{\text{pert}} = \left(\frac{m_*}{F M_{\text{ch}}} \right)^{\frac{1}{3}} \times 1.5 r_{\text{crit}}, \quad (12)$$

where m_* is the mass of a particle and M_{ch} the total mass in the chain. The parameter F controls the accuracy of the calculation of forces on the chain. Typically, $F = 10^{-6}$ is used. In principle r_{pert} should be proportional to r_{ch} . However, r_{ch} can sometimes change significantly during a chain step and it turned out that using $1.5 r_{\text{crit}}$ results in a much smaller integration error (the additional factor of 1.5 is due to the condition for particles to leave the chain). It also allows the perturber list to be re-used for several steps making the algorithm more efficient. Perturber particles act on the resolved chain as described below.

The force on the COM particle is calculated (6) in two steps. First, the force of the non-perturbers (i.e. particles outside of r_{pert}) on the COM particle is computed. This is done by loading the COM particle to the GRAPE and setting the masses of all perturber particles to zero at the same time. Then, a standard GRAPE call is used to compute the force, and the masses of the perturbers are set back to normal. In the second step, the forces of the perturbers on each chain particle are computed on the host. (In our applications, the number of perturbers is usually less than 100. Some problems may require a much larger number of perturbers, in which case it would be more efficient to use the GRAPE to do this force calculation as well.) The force on the individual chain particles is summed up according to

$$\mathbf{a}_{\text{COM,pert}} = \frac{1}{M_{\text{ch}}} \sum_{i_{\text{ch}}}^{N_{\text{ch}}} m_{i_{\text{ch}}} \mathbf{a}_{i_{\text{ch}}} \quad (13)$$

to give the total force on the COM particle (and likewise for the force derivatives).

In the next step (7), the chain particles are advanced for one system time step (which is the shortest time step needed by a non-chain particle and ideally longer than the shortest regular time step of the chain particles). This is achieved by sending the masses, positions and velocities of the chain and perturber particles plus the forces and force derivatives of the perturbers to ARCHAIN. The COM of the chain can change during this step because the chain is perturbed but any change is subtracted at this point.

Now a predictor-corrector step is made for the COM particle (step 8). Using the force calculated in step (6), position and velocity are predicted with equation (2), and these are then used to recompute the force on the COM particle in the same way as described above. The corrected position and velocity can then be calculated by equation (5).

The new position of the COM particle, together with the new positions and velocities of the chain particles calculated in the chain (7) can be used to resolve the chain, thus the true positions and velocities at the end of the current time step can now be written to the memory and GRAPE (including the COM particle). With the resolved chain it is now possible to compute the forces for the active particles. This again is done in two steps

for particles outside and inside of $r_{\text{res}} = F^{-1/3}r_{\text{ch}}$: First all active particles outside of r_{res} are integrated with the chain particles replaced by the COM particle. Then the active particles inside r_{res} are integrated seeing the resolved chain and not the COM particle. This is done by removing the COM particle from the GRAPE and by setting the masses of the chain particles back to normal.

Finally, a new time step can be computed for all active particles (note that the chain particles are not counted as active but everything in the chain is integrated in every step nonetheless). Positions and velocities are also updated on both the host and the GRAPE. Then, the integration can continue with the next step (going back to (2)).

If the chain is already active at the beginning of the time step, non-chain particles are checked to see whether they have entered the chain. A particle enters the chain if its distance to the chain COM is smaller than the chain radius r_{crit} . Any particle that enters the chain is, if needed, synchronized to t_{sys} first. Particles leave the chain if their distance to the COM becomes larger than $1.5r_{\text{crit}}$. The factor of 1.5 ensures that particles do not enter and leave the chain too often (to avoid the overhead associated with extra internal initialization each time chain membership is changed). A particle leaving the chain has its force, derivative and time step initialized and this information is sent to the GRAPE when the mass of this particle is set back to normal. The initialization of the time step is particularly important: errors are easily introduced into the integration if the time step is chosen too large. We use Eq. (1) with a rather small value for η_s , e.g. $\eta_s = 10^{-2}\eta$.

The search of perturber particle in step (5) is computationally rather expensive and is therefore not done in every step. A parameter Δt_{pert} is used to determine how often the list of perturbers is renewed (note that only the list of perturbers is unchanged for some time, current position etc. are still used within the chain). In addition, the perturber list is renewed whenever chain membership is changed. Also, the force on the COM particle only needs an update if the chain membership has changed.

Finally, an extra GRAPE call is needed to compute the potential for chain particles if at the end of a step if output of energies, etc. is required.

3. RESULTS OF PERFORMANCE TESTS

We tested the performance of the hybrid code using various realizations of a model designed to mimic the density profile of the star cluster around the Milky Way supermassive black hole (Fig. 1). The model has a mass density profile

$$\rho(r) = \rho_0 \left(\frac{r}{R_e} \right)^{-3/2} \exp \left[-b(r/R_e)^{1/n} \right]. \quad (14)$$

This is a $\rho \sim r^{-3/2}$ power-law near the center, similar to what is observed in the inner ~ 0.1 pc of the Milky Way (Schödel et al. 2007). An Einasto-like truncation was applied to give the model a finite total mass; the Einasto index was $n = 2$ and we adjusted b such that the truncation begins at a radius of $\sim 0.1R_e$. The total mass in stars was fixed to be equal to that of the BH particle, i.e. all “star” particles have mass $m = M_\bullet/N$.

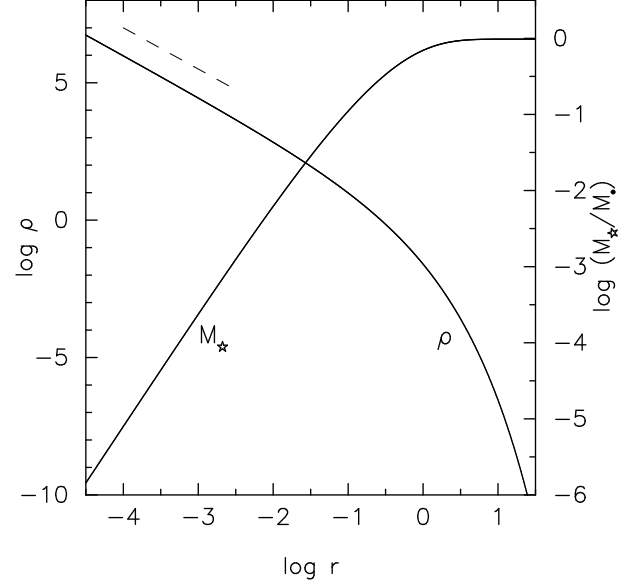


FIG. 1.— Density and mass profiles of the model used in the performance tests. The density obeys $\rho \propto r^{-1.5}$ near the center (dashed line) and is truncated via Einasto’s law beyond $r = 0.1$. The total mass in stars equals that of the “black hole” particle. This model can be roughly scaled to the Galactic center star cluster by setting the length unit to 1 pc and the total stellar mass to $3 \times 10^6 M_\odot$.

Henceforth units are adopted such that $G = M_\bullet = R_e = 1$; the model can be scaled approximately to the Galactic center by setting the length unit to 1 pc and the mass unit to $3 \times 10^6 M_\odot$, making the unit of time $\sim 10^4$ yr. Initial positions and velocities for the N “star” particles were generated by first computing the unique, isotropic phase-space distribution function $f(E)$ that reproduces the adopted $\rho(r)$ in the combined potential of the BH and the stars, then generating positions and velocities via Monte-Carlo sampling from ρ and f . Unless otherwise specified, performance tests were carried out on single nodes of `gravitySimulator`, a 32-node cluster with a GRAPE6-A card on each node (Harfst et al. 2007).

Figure 2 shows the integration time as a function of η for various N and for fixed $r_{\text{crit}} = 4 \times 10^{-4}$. For this value of r_{crit} , the typical number of particles in the chain, at any given time, is roughly linear in the particle number. The figure shows that, in this case, the scaling with the number of particles is approximately N^2 meaning that the total execution time is dominated by integration of particles outside the chain.

Figures 3 and 4 show the energy conservation and elapsed time for integrations until $t = 1$ for the case $N = 10^4$ and for various values of η , the accuracy parameter in the Hermite integrator (eq. 1), and r_{crit} , the maximum distance from the black hole at which a particle enters the chain (eq. 11b); t_{crit} (eq. 11b) was fixed at 5×10^{-5} and post-Newtonian terms were not included. (Including the PN terms was found to affect the speed of the code only very slightly; they were omitted in order to simplify the discussion of energy conservation.) Also shown is the performance of φ GRAPE without the regularized chain. The figures show the expected scaling of the Hermite scheme with the accuracy parameter: time steps increase linearly with η making the integra-

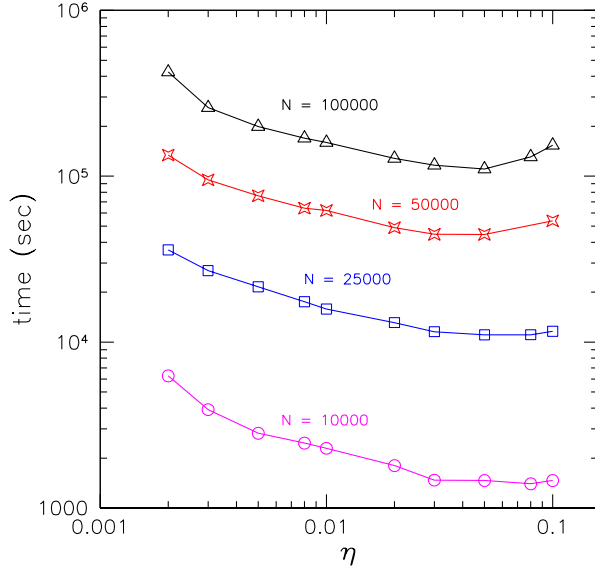


FIG. 2.— Elapsed time as a function of N and η in integrations until time $t = 1$, and with $r_{\text{crit}} = 4 \times 10^{-4}$.

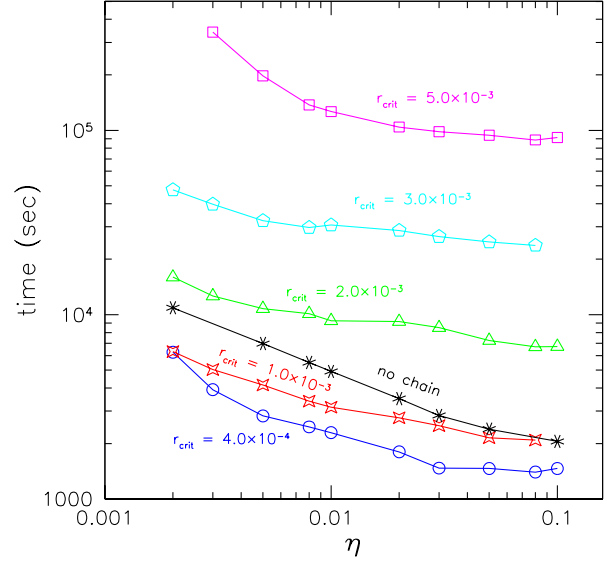


FIG. 4.— Elapsed time for the integrations of Fig. 3.

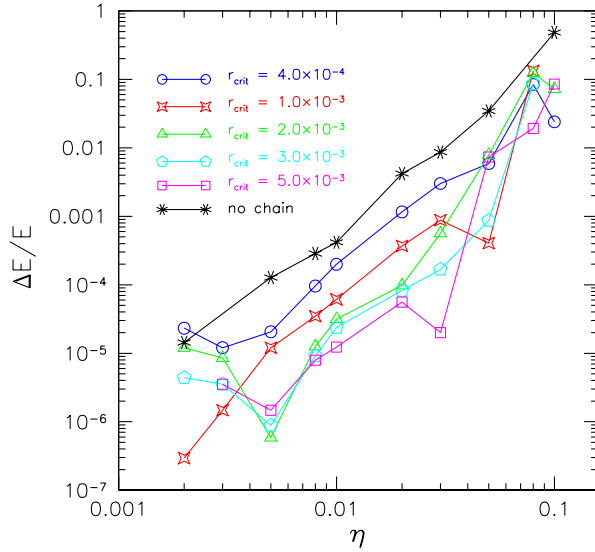


FIG. 3.— Energy conservation in integrations until $t = 1$ ($\sim 10^4$ yr) of the model illustrated in Fig. 1 with 10^4 particles. Black line (asterisks) are for φ GRAPE without the regularized chain.

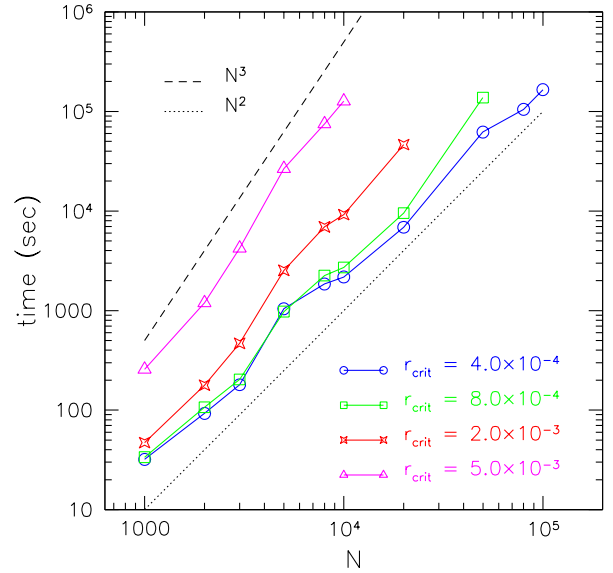


FIG. 5.— N -dependence of the elapsed time for integrations until $t = 1$ of the model in Figure 1, with $\eta = 0.01$. As the mean number of particles in the chain increases, the N -scaling changes from $\sim N^2$ (dotted line) to $\sim N^3$ (dashed line).

tion faster and less accurate. For a fourth-order scheme, the relative energy error scales as $\sim dt^5 \sim \eta^{5/2}$, though in the case of the hybrid code the relation is modified by the presence of the chain. Energy conservation generally improves for larger values of r_{crit} , as more and more particles are removed from the N -body integration and are treated more accurately in the chain. The integration time increases rapidly with r_{crit} reflecting the $\sim n_{\text{ch}}^3$ dependence of the chain. Nevertheless it is clear that for *all* values of η , there exist values of r_{crit} such that the hybrid code is both more accurate, *and faster*,

than φ GRAPE alone. This is presumably because the additional computational overhead associated with the regularization scheme is more than compensated for by the longer mean time steps of particles outside the chain.

The N -scaling of the integration time is more apparent in Figure 5. When r_{crit} is small, most of the computation is spent on the non-chain particles and the performance scales as $\sim N^2$. As r_{crit} increases, so does the typical number n_{ch} of particles in the chain, and the N -scaling of the total integration time changes to $\sim n_{\text{ch}}^3 \sim N^3$. Along the line $r_{\text{crit}} = 2 \times 10^{-3}$ in Figure 5, which roughly marks

the transition from an $\sim N^2$ to an $\sim N^3$ scaling, the mean fraction n_{ch}/N of particles in the chain varies from $\sim 3 \times 10^{-4}$ to $\sim 7 \times 10^{-4}$. If we postulate a performance model in which the total integration time is simply the sum of the time spent on particles in the chain, $t_{\text{ch}} = An_{\text{ch}}^3$, plus the time spent on particles outside the chain, $t_N = BN^2$, then the fraction $(n_{\text{ch}}/N)_{\text{crit}}$ at which the chain begins to dominate the total time should scale as $N^{-1/3}$. We did not attempt to verify this prediction in detail, but if we adopt $(n_{\text{ch}}/N)_{\text{crit}} \approx 5 \times 10^{-4}$ at $N = 10^4$, the model predicts $(n_{\text{ch}}/N)_{\text{crit}} \approx 0.01N^{-1/3}$. This relation can be taken as defining the effective upper limit to the number of particles to include in the chain; for $N = 10^6$, $n_{\text{ch,crit}} \approx 100$.

The results presented in this section constitute a particularly severe test of the code, since all of the particles are moving, at all times, in the essentially Keplerian potential of the central mass. In many other applications, the sphere of influence of the massive particle(s) would only include a fraction of the other particles in the simulation, and a choice of r_{crit} could be made that included all the particles in this region without forcing n_{ch} to unreasonable values.

4. APPLICATIONS

4.1. Evolution of Orbits near the Galactic Center Black Hole

AR-CHAIN conserves the Keplerian elements of unperturbed two-body orbits with extremely high precision, even for arbitrarily large mass ratios, and this fact makes the hybrid code uniquely suited to investigating the detailed effects of perturbations on the orbits of individual stars around the galactic center supermassive black hole (SMBH).

We illustrate this using the collisionally relaxed, multi-mass model of Hopman & Alexander (2006b) (hereafter the “HA06 model”). This model has four components in addition to the SMBH: main sequence (MS) stars, $m = 1M_{\odot}$; white dwarfs (WD), $m = 0.6M_{\odot}$; neutron stars (NS), $m = 1.4M_{\odot}$; and stellar-mass black holes (BH), $m = 10M_{\odot}$. The HA06 model was derived as a steady-state solution of the isotropic, orbit-averaged Fokker-Planck equation assuming a SMBH mass of $3 \times 10^6 M_{\odot}$, and including an approximate term representing loss of stars into the tidal disruption sphere. The contribution of the stars to the gravitational potential was ignored, making the solution valid only within the SMBH’s influence radius, $r \lesssim 1$ pc. The three lighter species (which dominate the density at most radii) have $\rho \sim r^{-\gamma}$, $1.4 \lesssim \gamma \lesssim 1.5$, $r \gtrsim 3$ mpc while the heavier BHs have a steeper profile, $\gamma \approx 2$. Detailed density profiles for the four species were kindly provided by T. Alexander. We modified the HA06 model by imposing a steep truncation like that of Figure 1 to the density of each species beyond $r = 0.1$ pc, then computed the self-consistent isotropic phase-space density $f_i(E)$, $i = 1, \dots, 4$ corresponding to each species from the truncated $\rho_i(r)$ profiles using Edington’s formula. Finally, Monte-Carlo positions and velocities were generated from the ρ_i and f_i . The total number of objects of all types was found to be $\sim 75,000$, with $\sim 10^3$ objects (mostly MS stars) within 0.01 pc; the latter number is consistent with the value given in Table 1 of Hopman & Alexander (2006b). Hereafter, we refer

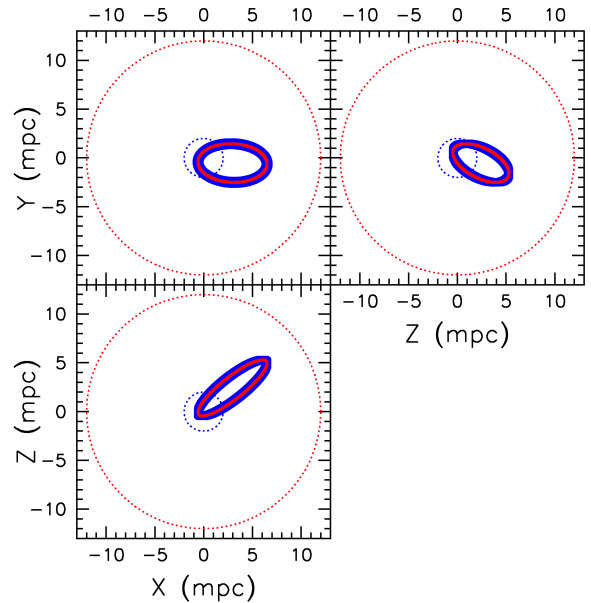


FIG. 6.— Orbit of the galactic center star S0-2 over a time of 100 yr in the case of $r_{\text{crit}} = 2$ mpc (blue) and $r_{\text{crit}} = 12$ mpc (red). The total number of stars in these integrations was 10^3 and post-Newtonian terms were not included.

collectively to stars and stellar remnants in the N -body simulation simply as “stars.”

The non-zero masses of the stars cause the N -body gravitational potential to deviate slightly from the fixed Keplerian potential of the SMBH, and the resultant perturbations cause the orbital elements of any single (“test”) star to evolve.

As test stars, we included five particles with orbital elements corresponding to the five, shortest-period S stars observed near the galactic center: S0-1, S0-2, S0-16, S0-19, and S0-20. Masses of these five stars were set to $15M_{\odot}$ and initial positions and velocities were determined at year 2000 AD using the Keplerian orbital elements given in Table 3 of Ghez et al. (2005). (Initial velocities of the S-stars were adjusted, at fixed a and e , to account for the slightly different values of M_{BH} assumed by Hopman & Alexander (2006) and Ghez et al. (2005).) These stars are being constantly monitored and deviations of their orbits from closed Keplerian ellipses might be used to test various hypotheses about the distribution of matter near the SMBH, or as a test of general relativity (e.g. Fragile & Mathews 2000; Rubilar & Eckart 2001; Weinberg et al. 2005; Zucker et al. 2006; Will 2008).

The total number of stars in the HA06 model contained within the S-star orbits is $\gtrsim 10^3$, too large for all of them to be included in the chain at one time; this necessitates a choice of r_{crit} such that the S-stars will pass in and out of the chain in each orbit. We first verified that passage through r_{crit} did not in itself introduce significant changes in the orbital elements. Figures 6 and 7 show the results of one such set of tests, which followed the orbit of S0-2 for two different values of r_{crit} : $r_{\text{crit}} = 2$ mpc and $r_{\text{crit}} = 12$ mpc, compared with the semi-major axis length of 4.5 mpc. The total number of stars in this test was set to 10^3 in order that all particles within the largest r_{crit} could be included in the chain without exceeding a chain membership of ~ 100 . Post-Newtonian terms were

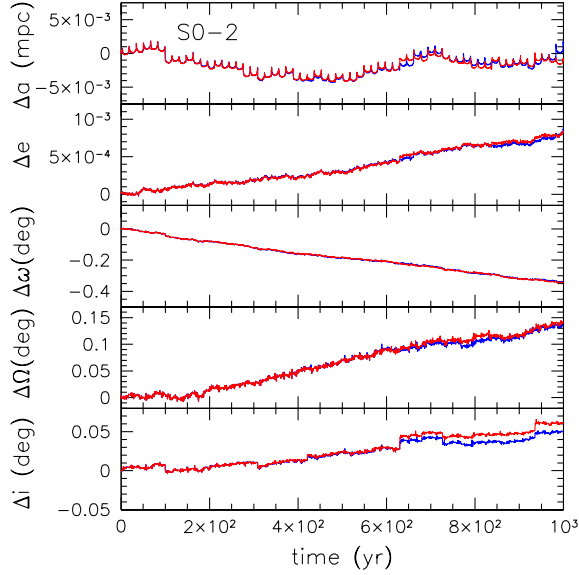


FIG. 7.— Evolution of the orbital elements of star S0-2 in integrations with $N = 10^3$ stars and $r_{\text{crit}} = 2$ mpc (blue) and $r_{\text{crit}} = 12$ mpc (red).

not included. Figure 7 shows the evolution of the five classical elements of the Keplerian orbit of S0-2 over a time span of 10^3 years. There are only slight differences between the two runs, verifying that entrance into, or departure from, the chain does not significantly influence the orbit.

The timescale for apoastron precession in the S-stars (represented by $\Delta\omega$ in Fig. 7) is $\gtrsim 10^5$ yr (e.g. Weinberg et al. 2005). On shorter timescales, the angular momentum of stars like S0-2 should evolve approximately linearly with time due to the (essentially fixed) torques resulting from finite- N departures of the overall potential from spherical symmetry (Rauch & Tremaine 1996).

This evolution is illustrated for all the S-stars in Figure 8. The blue lines in that figure are from an integration that used the complete set of $N = 7.5 \times 10^4$ stars in the Monte-Carlo realization of the HA06 model, and $r_{\text{crit}} = 0.8$ mpc; also shown are integrations that used randomly-chosen subsets of 10^4 stars ($r_{\text{crit}} = 2$ mpc) and 10^3 stars ($r_{\text{crit}} = 10$ mpc) from this model. Plotted in Figure 8 are the two Keplerian elements $(i, \Omega) = (\text{inclination, right ascension of ascending node})$ that measure the orientation of the orbital planes. These angles would remain precisely constant in any spherical potential and their evolution is due entirely to finite- N departures of the potential from spherical symmetry. The two angles are related to the Cartesian components of the angular momentum via

$$L_x = L \sin i \sin \Omega, \quad (15a)$$

$$L_y = -L \sin i \cos \Omega, \quad (15b)$$

$$L_z = L \cos i. \quad (15c)$$

Simple arguments (Rauch & Tremaine 1996) suggest that orbital inclinations should evolve in this regime ap-

proximately as

$$\Delta(i, \Omega) \approx A \frac{m}{M_\bullet} N^{1/2} \frac{t}{P} \quad (16a)$$

$$\approx A \frac{m}{2\pi} \left(\frac{GN}{M_\bullet a^3} \right)^{1/2} t \quad (16b)$$

where m is a typical perturber mass, N is the number of stars within a sphere of radius a , the semi-major axis of the test star, and $P(a)$ is the (Keplerian) orbital period. The coefficient A is thought to be of order \sim a few but is otherwise not well known (Rauch & Tremaine 1996). We evaluated equation (16b) numerically for the $N = 75K$ model and found that the dominant contribution to the torques is predicted to come from the BH particles; the predicted change in orientation of a test star over 10^4 yr, for $A = 1$, is $\sim 0.5^\circ$ for $a = 10$ mpc increasing to $\sim 1^\circ$ for $a = 2$ mpc. This is quite consistent with Figure 8 if $2 \lesssim A \lesssim 3$. The dependence of the evolution on N in Figure 8 is also consistent with the $N^{1/2}$ prediction of equation (16).

These examples suggest that the hybrid code will be an effective tool for studying so-called “resonant relaxation” of orbits near a supermassive black hole (e.g. Hopman & Alexander 2006a).

4.2. Inspiral of an IMBH into the Galactic Center

As a second test problem, we used φ GRAPECH to follow the inspiral of an intermediate-mass black hole (IMBH) into the Galactic SMBH. The multi-mass stellar cusp model described in the previous sub-section was again used, with $N = 75K$. The second black hole was given a mass of 10^{-3} times that of the SMBH, or $3 \times 10^3 M_\odot$; its initial orbit around the SMBH had semi-major axis 0.1 mpc and its eccentricity was 0.9. This initial separation is of the same order as the so-called hard-binary separation a_h at which inspiral due to dynamical friction alone would be expected to stall (e.g. Gualandris & Merritt 2007, eq. 4.1). The large eccentricity was chosen primarily to accelerate the inspiral. For constant e , the time required for gravitational wave emission to bring the two black holes together is (e.g. Merritt & Milosavljević 2005, eq. 7)

$$t_{\text{GW}} = \frac{5}{256 F(e)} \frac{c^5}{G^3} \frac{a(0)^4}{\mu M_{12}^2} \quad (17a)$$

$$\approx \frac{5}{256 F(e)} \frac{c^5 a(0)^4}{q (GM_1)^3} \quad (17b)$$

where $M_{12} = M_1 + M_2 \approx M_1$ is the total mass of the binary, $\mu = M_1 M_2 / M_{12} \approx q M_1$ when $q = M_2 / M_1 \ll 1$, and $F(e) = 335$ for $e = 0.9$. This can be written

$$t_{\text{GW}} \approx 6.4 \times 10^3 \text{ yr} \left(\frac{a(0)}{0.1 \text{ mpc}} \right)^4 \left(\frac{q}{10^{-3}} \right)^{-1} \left(\frac{M_1}{3 \times 10^6 M_\odot} \right)^{-3} \quad (18)$$

The actual inspiral time is expected to differ slightly from this value since (a) the orbital eccentricity will change with time due to the dissipative effect of the PN terms, and (b) in the presence of stars, gravitational encounters will exchange energy and angular momentum with the binary.

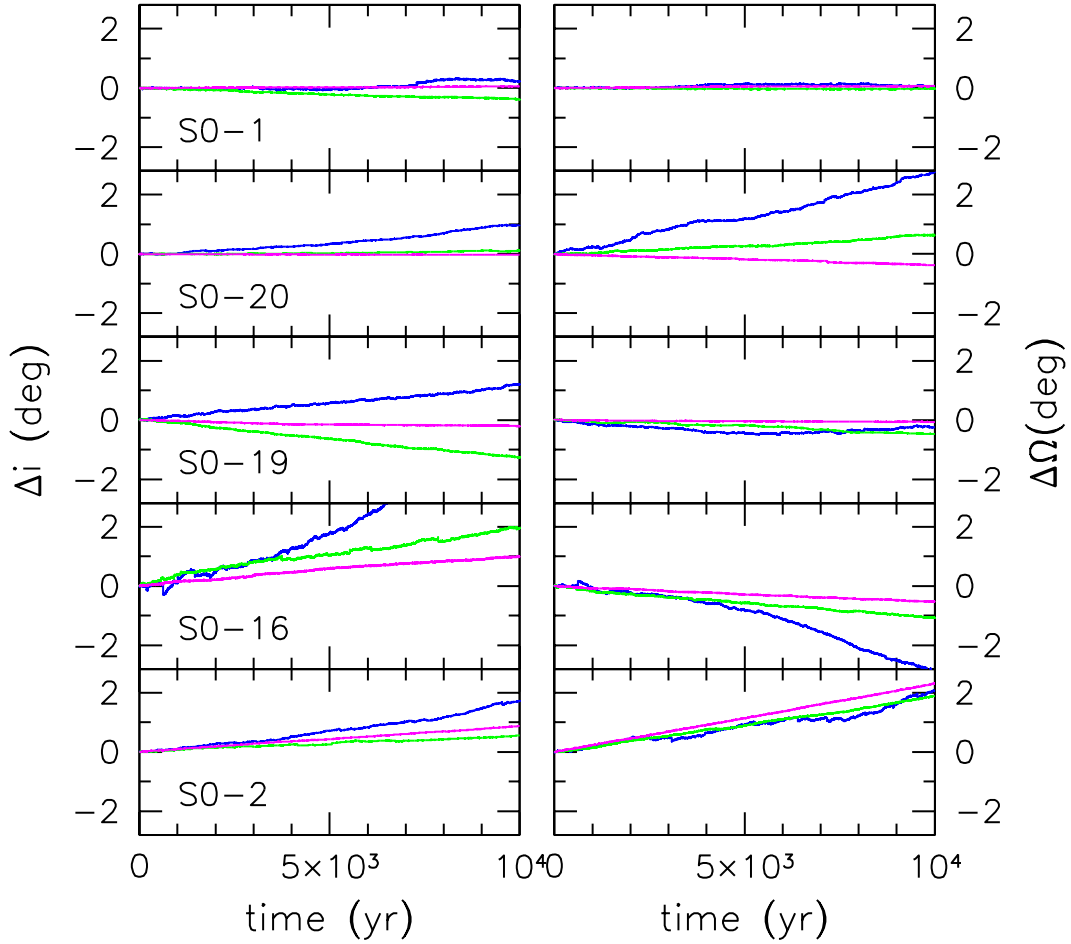


FIG. 8.— Evolution of the orbital plane of the S-stars over a time span of 10^4 years in integrations with different particle numbers: $N = 10^3$ (magenta), $N = 10^4$ (green), $N = 7.5 \times 10^4$ (blue). The left panels show the inclination angle i while the right panels show position angle of the nodal point Ω , as defined in Ghez et al. (2005).

The integration used $r_{\text{crit}} = 0.8$ mpc, $\eta = 0.01$ and $\epsilon = 10^{-5}$ mpc. It required a time of 60 hr on one node of the GRAPE cluster.

The evolution of the distance between the IMBH and the SMBH is presented in Figure 9. As a comparison, the same evolution is shown for an integration in which ARCHAIN was used to follow the binary in the absence of stars. In this case, the stars have no significant effect on time scale for inspiral, which occurs in ~ 6000 yr, in good agreement with Eq. 18.

Figure 10 (top panel) shows the trajectory of the IMBH over a time of 4.5 yr, which roughly corresponds to the time for ω to precess 360° twice (bottom panel). The longitude of the periastron is predicted to advance by an amount

$$\Delta\omega \approx 0.15^\circ (1 - e^2)^{-1} \left(\frac{M_{\text{BH}}}{3 \times 10^6 M_\odot} \right) \left(\frac{\text{mpc}}{a} \right) \quad (19)$$

each orbital period; this corresponds to $\sim 8^\circ$ per revolu-

tion for $a = 0.1$ mpc and $e = 0.9$.

In the absence of stars, evolution of the IMBH/SMBH binary would take place in a fixed plane, i.e. i and Ω would remain constant. In the presence of stars, however, deviations of the potential from spherical symmetry cause the orientation of the binary to change with time (Merritt 2002). The evolution of the Keplerian elements of the binary can be seen in Figure 11, which shows a substantial change in the binary's orbital plane during the course of the inspiral. Similar evolution has been observed in other N -body studies (e.g. Milosavljević & Merritt 2001; Baumgardt et al. 2006).

We also show the evolution of the orbits of the three innermost S-stars in Figure 12. The periastron distance of S0-16 is 0.2 mpc, roughly equal to the initial apoapse distance of the IMBH. This orbit evolves strongly due to interactions with the IMBH. The semi-major axis increases by a factor of ~ 4 and the eccentricity increases almost to one. If the inspiral were prolonged, e.g. by

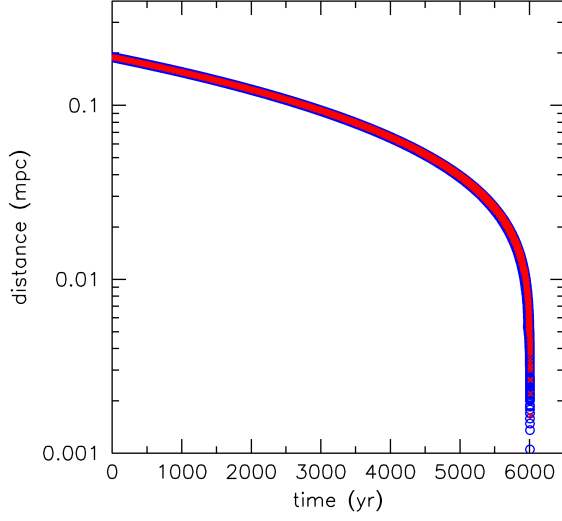


FIG. 9.— Evolution of the distance between the IMBH and the SMBH over the inspiral time. The blue points refer to the simulation containing $N = 75K$ stars while the red points refer to a simulation of the black hole binary in isolation.

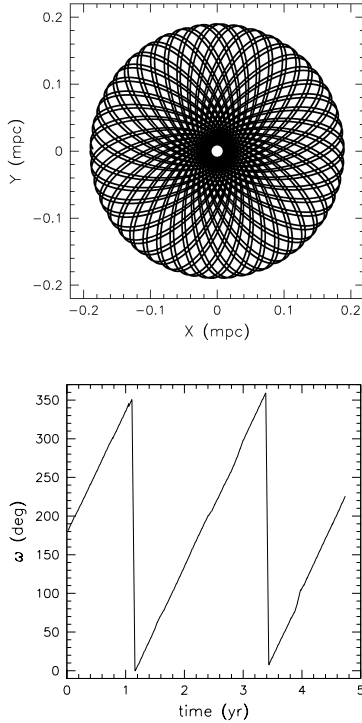


FIG. 10.— (Top) Trajectory of the IMBH over a time of 4.5 yr, showing precession of the periastron due to the PN terms. (Bottom). Periastron advancement for the IMBH orbit.

making the IMBH orbit less eccentric, Fig. 12 suggests that this star and star S0-2 might be ejected completely after a few tens of thousands of years.

The binary ejects stars that interact strongly with it and such ejections are a possible source of the so-called hyper-velocity stars (Brown et al. 2006). Figure 13

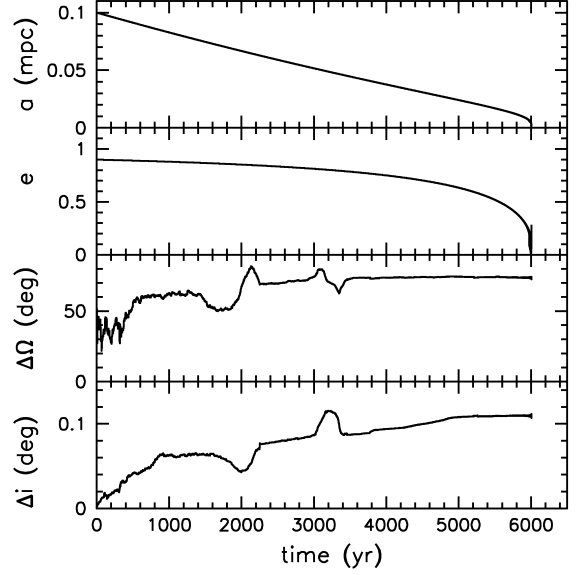


FIG. 11.— Evolution of the Keplerian elements of the black hole binary over the full inspiral time.

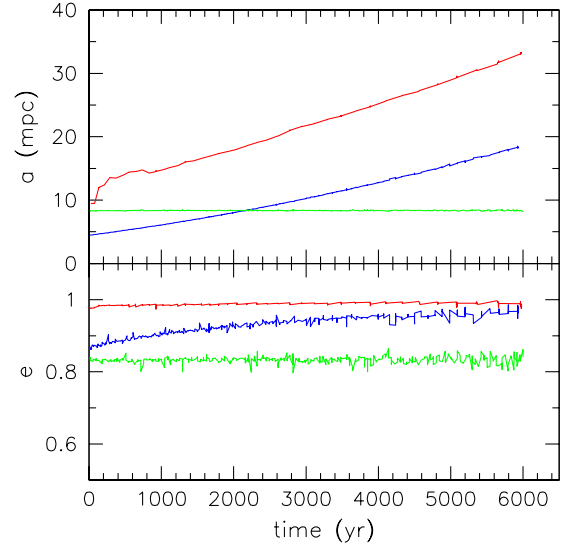


FIG. 12.— Orbital elements of the S-stars S0-2 (blue), S0-16 (red) and S0-19 (green) over a time of 6000 yr.

shows the distribution of ejection velocities for stars unbound to the SMBH at the end of the IMBH inspiral. The peak of the distribution is at $V_{\text{peak}} \sim 300 \text{ km s}^{-1}$. Interestingly, about 30% of the ejected stars have velocities $\gtrsim 700 \text{ km s}^{-1}$, i.e. large enough to escape the bulge and reach the Galactic halo as hyper-velocity stars. About 150 stars are ejected during the inspiral, which results in an average ejection rate of $\sim 20000 \text{ Myr}^{-1}$. This rate is somewhat higher than observed in simulations that start with a more separated binary (e.g. Baumgardt et al. 2006), presumably because most of the ejections we see are from stars on orbits that intersect

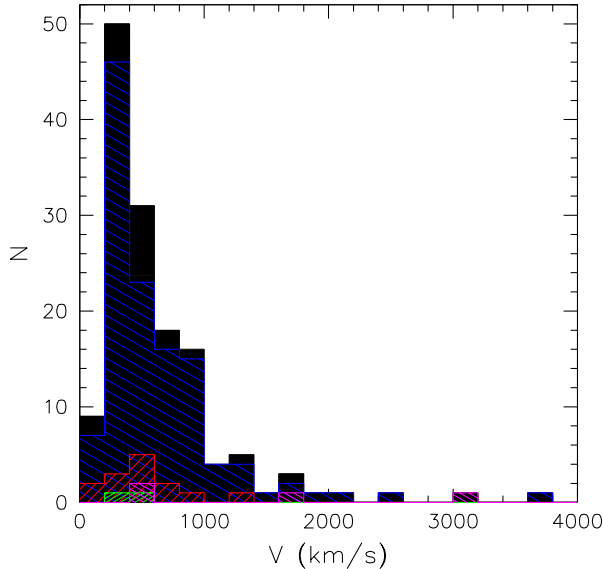


FIG. 13.— Velocity distribution for stars and stellar remnants escaping from the SMBH at the end of the IMBH inspiral. The distribution for all escapers is presented in black, while the curves for individual species are: main-sequence (blue), white-dwarfs (red), neutron stars (green), black holes (magenta).

the binary at time zero, and many of these stars would have been ejected at earlier times. Most of the escapers are main-sequence stars, which is not surprising given their dominance in the cluster. Nonetheless, a handful of stellar mass black holes are ejected with velocities up to 3000 km s^{-1} .

5. SUMMARY

We have described a new N -body code, called φ GRAPECH, designed for simulations of the central regions of galaxies containing supermassive black holes. Based on the serial implementation of φ GRAPE, the new code incorporates the algorithmic chain regularization scheme to treat orbits near the central black hole

with high precision. Post-Newtonian terms are included up to PN2.5 order.

In performance tests of the new code, we find that the new hybrid code achieves better energy conservation in less computation time when compared to the standard pure 4th-order Hermite integration scheme. A simple performance model indicates that the computation time for particles in the chain will dominate the total computation time if the fraction of chain particles exceeds a certain limit. This limit is at about 100 chain particles for a total number of particles of one million particles.

We then apply our new hybrid code to a model of the Galactic center that includes a supermassive black hole and four different stellar mass components. In addition, the five shortest-period S-stars were also included. We show that the orbits of S-stars are integrated with very high precision. We were able to measure the change in the orbital plane of S-stars due the effect of the finite- N departures of the potential from spherical symmetry. The measured change is in very good agreement with theoretical predictions.

As a second application, we added an inspiraling intermediate-mass black hole to the model of the Galactic center. The time scale of the inspiral is unaffected by the stars and agree well with theoretical predictions. However, the orbital plane of the inspiral is changed by the stars. A number of stars are ejected from the center and a significant fractions has velocities large enough to reach the Galactic halo as hyper-velocity stars.

The authors are very much indebted to S. Aarseth and R. Spurzem for their many helpful suggestions about how to incorporate AR-CHAIN in the N -body code. We are also grateful to T. Alexander for kindly providing the details of the galactic center model used in §4. SH is supported by the NWO Computational Science STARE project 643200503. AG and DM were supported by grants AST-0420920 and AST-0437519 from the NSF, grant NNX07AH15G from NASA, and grant HST-AR-09519.01-A from STScI.

REFERENCES

- Aarseth S. J., 1985, in Brackbill J. U., Cohen B. I., eds, *Multiple Time Scales* Direct methods for N -body simulations. p. 377
- Aarseth S. J., 2003a, *Ap&SS*, 285, 367
- Aarseth S. J., 2003b, *Gravitational N-Body Simulations*. ISBN 0521432723. Cambridge, UK: Cambridge University Press, November 2003.
- Aarseth S. J., 2007, *MNRAS*, 378, 285
- Baumgardt H., Gualandris A., Portegies Zwart S., 2006, *MNRAS*, 372, 174
- Baumgardt H., Makino J., Ebisuzaki T., 2004, *ApJ*, 613, 1133
- Brown W. R., Geller M. J., Kenyon S. J., Kurtz M. J., 2006, *ApJ*, 640, L35
- Eisenhauer F., Genzel R., Alexander T., Abuter R., Paumard T., Ott T., Gilbert A., Gillessen S., Horrobin M., Trippe S., Bonnet H., Dumas C., Hubin N., Kaufer A., Kissler-Patig M., Monnet G., Ströbele S., Szeifert T., Eckart A., Schödel R., Zucker S., 2005, *ApJ*, 628, 246
- Fragile P. C., Mathews G. J., 2000, *ApJ*, 542, 328
- Ghez A. M., Salim S., Hornstein S. D., Tanner A., Lu J. R., Morris M., Becklin E. E., Duchêne G., 2005, *ApJ*, 620, 744
- Gualandris A., Merritt D., 2007, *ArXiv e-prints*, 708
- Harfst S., Gualandris A., Merritt D., Spurzem R., Portegies Zwart S., Berczik P., 2007, *New Astronomy*, 12, 357
- Hopman C., Alexander T., 2006a, *ApJ*, 645, 1152
- Hopman C., Alexander T., 2006b, *ApJ*, 645, L133
- Kustaanheimo P., Stiefel E., 1965, *J. Reine Angew. Math.*, 218, 204
- Löckmann U., Baumgardt H., 2008, *MNRAS*, 384, 323
- Makino J., Aarseth S. J., 1992, *PASJ*, 44, 141
- Makino J., Fukushima T., Koga M., Namura K., 2003, *PASJ*, 55, 1163
- Matsubayashi T., Makino J., Ebisuzaki T., 2007, *ApJ*, 656, 879
- McMillan S. L. W., 1986, *LNP Vol. 267: The Use of Supercomputers in Stellar Dynamics*, 267, 156
- Merritt D., 2002, *ApJ*, 568, 998
- Merritt D., Mikkola S., Szell A., 2007, *ApJ*, 671, 53
- Merritt D., Milosavljević M., 2005, *Living Reviews in Relativity*, 8, 8
- Mikkola S., Aarseth S., 2002, *Celestial Mechanics and Dynamical Astronomy*, 84, 343
- Mikkola S., Aarseth S. J., 1993, *Celestial Mechanics and Dynamical Astronomy*, 57, 439
- Mikkola S., Merritt D., 2006, *MNRAS*, 372, 219
- Mikkola S., Merritt D., 2007, *ArXiv e-prints*, 709
- Mikkola S., Tanikawa K., 1999a, *MNRAS*, 310, 745
- Mikkola S., Tanikawa K., 1999b, *Celestial Mechanics and Dynamical Astronomy*, 74, 287
- Milosavljević M., Merritt D., 2001, *ApJ*, 563, 34

- Preto M., Tremaine S., 1999, *AJ*, 118, 2532
Quinlan G. D., Hernquist L., 1997, *New Astronomy*, 2, 533
Rauch K. P., Tremaine S., 1996, *New Astronomy*, 1, 149
Rubilar G. F., Eckart A., 2001, *A&A*, 374, 95
Schödel R., Eckart A., Alexander T., Merritt D., Genzel R.,
Sternberg A., Meyer L., Kul F., Moulata J., Ott T.,
Straubmeier C., 2007, *A&A*, 469, 125
Sigurdsson S., Hernquist L., Quinlan G. D., 1995, *ApJ*, 446, 75
Weinberg N. N., Milosavljević M., Ghez A. M., 2005, *ApJ*, 622,
878
Will C. M., 2008, *ApJ*, 674, L25
Zare K., 1974, *Celestial Mechanics*, 10, 207
Zucker S., Alexander T., Gillessen S., Eisenhauer F., Genzel R.,
2006, *ApJ*, 639, L21